HQCNN: A Hybrid Quantum-Classical Neural Network for Medical Image Classification

Shahjalal, Jahid Karim Fahim, Pintu Chandra Paul*, Md Robin Hossain, Md. Tofael Ahmed, and Dulal Chakraborty

Department of Information and Communication Technology, Comilla University, Cumilla-3506, Bangladesh

Classification of medical images plays a vital role in medical image analysis; however, it remains challenging due to the limited availability of labeled data, class imbalances, and the complexity of medical patterns. To overcome these challenges, we propose a novel Hybrid Quantum-Classical Neural Network (HQCNN) for both binary and multi-class classification. The architecture of HQCNN integrates a five-layer classical convolutional backbone with a 4-qubit variational quantum circuit that incorporates quantum state encoding, superpositional entanglement, and a Fourier-inspired quantum attention mechanism. We evaluate the model on six MedMNIST v2 benchmark datasets. The HQCNN consistently outperforms classical and quantum baselines, achieving up to 99.91% accuracy and 100.00% AUC on PathMNIST (binary) and 99.95% accuracy on OrganAMNIST (multi-class) with strong robustness on noisy datasets like BreastMNIST (87.18% accuracy). The model demonstrates superior generalization capability and computational efficiency, accomplished with significantly fewer trainable parameters, making it suitable for data-scarce scenarios. Our findings provide strong empirical evidence that hybrid quantum-classical models can advance medical imaging tasks.

1 Introduction

Medical imaging has become an essential component of modern healthcare, enabling non-invasive visualization of internal anatomical structures and physiological processes. Techniques such as magnetic resonance imaging (MRI), computed tomography (CT), ultrasound, histopathology, and X-rays are routinely used to diagnose, monitor, and support treatment planning a wide range of diseases, including cancer, cardiovascular disorders, and organ-specific abnormalities [1]. With the proliferation of digital imaging in healthcare, there has been an exponential increase in the volume and complexity of medical image data. Manual analysis by radiologists or pathologists is labor-intensive, time-consuming, and subject to inter- and intra-observer variability [2]. These limitations have fueled the demand for automated, intelligent image classification systems capable of delivering fast, accurate, and consistent diagnostic support. In recent years, deep learning, particularly Convolutional Neural Networks (CNNs), has achieved remarkable success in medical image classification tasks [3, 4].

Classical Convolutional Neural Networks (CNNs) excel at automatically learning hierarchical representations from pixel-level data, surpassing traditional handcrafted feature-based methods [1, 4]. However, they face critical limitations in medical applications. They incur high computational costs during training and inference [5], though lightweight architectures like MobileNet and EfficientNet mitigate this for resource-constrained environments [5]. Their performance depends on large, annotated datasets, which are scarce in medical imaging [6]. CNNs struggle with robustness against noisy inputs, class imbalance, or ambiguous features common in clinical data, such as chest X-ray analysis [7, 3], although recent methods like confident learning offer partial solutions [8]. Their frequent over-parameterization increases overfitting risks, limiting generalization. Criti-

Shahjalal: shahjalalkhanrabbi@gmail.com
Pintu Chandra Paul* pintu@cou.ac.bd

cally, CNNs often lack interpretability, raising concerns about transparency in high-stakes medical applications, though explainable AI methods are emerging [9, 10].

These challenges are particularly evident when applying CNNs to multi-class medical classification tasks, where datasets may exhibit class imbalance, subtle inter-class variations, and limited sample sizes. To address these issues, emerging research has begun exploring the potential of quantum machine learning (QML), a field that combines quantum computing with classical AI techniques. Quantum systems, leveraging phenomena such as superposition and entanglement, offer advantages in representational capacity and data encoding in high-dimensional Hilbert spaces.

Quantum neural networks (QNNs), particularly variational quantum circuits (VQCs), have shown considerable promise in learning expressive, nonlinear transformations with fewer trainable parameters compared to classical deep neural networks [11, 12]. When integrated with classical convolutional architectures, hybrid quantum-classical neural networks (HQCNNs) form a robust framework for image classification by leveraging quantum properties such as superposition and entanglement to model intricate feature dependencies. Hybrid models reduce parameter complexity and improve generalization in low-data regimes by leveraging quantum expressivity. Notably, Fan et al. [13] demonstrated that an HQCNN with amplitude encoding significantly improved both classification accuracy and computational efficiency in Earth observation imagery, highlighting the potential of quantum-enhanced architectures in existing applications.

In this work, we propose a novel HQCNN model tailored for medical image classification. We incorporate a Fourier-inspired quantum attention mechanism into a hybrid architecture to address the existing challenges presented by MedMNIST datasets, such as class imbalance and multi-class structure. Our model is:

- Architecturally robust and modular for data-scarce scenarios in medical images
- Integrated seamlessly with classical PyTorch training pipelines via Pennylane's TorchLayer [14].

In this landscape, our proposed HQCNN model represents a practical and architecture-rich quantum machine learning system tailored for medical image classification. Unlike purely classical CNNs or standalone quantum models, our hybrid approach combines the strengths of both paradigms. Our main contributions are:

1. To propose a novel Hybrid Quantum-Classical Neural Network (HQCNN) architecture for multi-class medical image classification, applied to six benchmark datasets from the MedMNIST collection.

2. To integrate quantum state encoding, superpositional entanglement, and a Fourier-inspired attention mechanism, enabling effective feature extraction and robust classification performance even under constrained data conditions.

3. To evaluate the performance of our HQCNN model using different evaluation metrics such as accuracy and AUC scores.

4. To provide empirical evidence that hybrid-classical models offer improved classification efficiency compared to the classical deep learning models in medical imaging tasks.

The rest of the paper is formatted as follows: Section 2 presents the reviews of related work in the literature. Section 3 describes the proposed HQCNN model architecture. Section 4 presents experimental results and discussion. Finally, Section 5 concludes this paper with future directions.

2 Related Work

Recent advances in quantum machine learning (QML) and classical deep learning have substantially reshaped the landscape of medical image classification. While convolutional neural networks (CNNs) have demonstrated high accuracy in diverse medical imaging tasks, the emergence of quantum neural networks (QNNs) and hybrid quantum-classical architectures offers promising alternatives, particularly under constraints such as limited data, noisy labels, and hardware efficiency. This section presents a comprehensive review of classical models, quantum circuits, and hybrid frameworks, followed by a discussion of the research gap that our work aims to address.

CNN-based models have long been the backbone of medical image analysis due to their ability to extract spatial and hierarchical features. Architectures such as ResNet [15], DenseNet [16], and MobileNet [5] have been adapted for disease classification, organ detection, and segmentation. [1] provided an exhaustive survey of CNN applications across radiology, histopathology, and ophthalmology.

The MedMNIST v2 benchmark [6] has established a standardized platform for evaluating lightweight medical image classifiers across various modalities. Baseline models such as shallow ResNet variants achieved competitive performance but exhibit sensitivity to class imbalance and low-resolution inputs. Models like MedViT [17] and AutoKeras [18] have further explored architecture search and Transformer-based adaptations for biomedical tasks. [19] benchmarked MedMNIST using a 127-qubit IBM quantum computer, demonstrating the feasibility of pure QNNs with hardware-efficient circuits and advanced error mitigation.

Despite their widespread adoption and strong empirical performance, classical deep learning models often exhibit significant limitations. These include a heavy dependence on large, high-quality datasets, pronounced sensitivity to class imbalance and label noise [8, 7], high computational requirements, and limited model interpretability, an issue that is particularly critical in high-stakes medical decision-making scenarios [9, 10].

Recent studies demonstrate the application of hybrid quantum neural networks across various medical imaging modalities. [20] showcased a quantum algorithm that outperformed traditional deep learning models in classifying COVID-19 CT scan images, emphasizing the importance of image processing techniques in achieving high diagnostic accuracy. Similarly, [21] explored circuit-based hybrid quantum convolutional neural networks (QCNNs) for remote sensing imagery, illustrating how quantum layers integrated into classical CNN architectures can serve as effective image classifiers.

QNNs based on Variational Quantum Circuits (VQCs) have emerged as expressive models capable of representing complex nonlinear functions using a limited number of qubits [22]. These circuits leverage quantum properties such as superposition, entanglement, and interference to encode and process data in high-dimensional Hilbert spaces.

[11] introduced Quantum Convolutional Neural Networks (QCNNs), demonstrating the feasibility of hierarchical quantum architectures. [12] proposed data re-uploading to boost model expressivity. However, many existing QNNs are limited to synthetic datasets like MNIST and lack scalability or generalization to existing medical data.

[23] explored quanvolutional layers, and [24] proposed a hybrid quantum-classical QCNN model incorporating a novel quantum perceptron and an optimized circuit design for 4-class MNIST classification, demonstrating performance comparable to classical CNNs and suggesting further improvements through qubit-based architectures suited for the NISQ era.

Hybrid architectures, which combine classical layers with quantum circuits, have gained traction for overcoming the limitations of Noisy Intermediate-Scale Quantum (NISQ) devices. These models embed quantum layers into CNN pipelines to improve expressiveness and reduce parameterization while remaining trainable via backpropagation [25].

[26] proposed a distributed QCNN for 8-qubit convolution using only 5 physical qubits, improving scalability. [27] presents a hybrid quantum-classical CNN model for detecting COVID-19 using chest X-ray images. They utilized a collection of 5445 chest X-ray images for evaluation. The model demonstrated effective performance in distinguishing COVID-19 from other conditions.

[28] explored quanvolutional layers, addressed the computational challenges faced in image classification by proposing quantum machine learning models that leverage quantum mechanics for more effective processing of large visual datasets. [29] demonstrated performance stability using momentum-based hybrid optimization on brain MRI datasets. [30] proposed a hybrid quantum-classical CNN using separable convolutions followed by a quantum layer for classifying brain tumors on MRI. [31] introduced two quantum methods: quantum-assisted neural networks and orthogonal QNNs. They show comparable accuracy to classical networks on retinal fundus and chest X-rays, both in simulation and real quantum hardware. [32] introduced param-

eterized quantum circuits (PQCs) for both data encoding and quantum neural networks (QNNs), using layered U3 gates and entanglement strategies to enable multiclass classification via quantum expectation measurements.

A number of systematic reviews have explored the broader landscape of quantum machine learning (QML) in medical applications. [33] surveyed recent advancements in QML for medical image analysis, emphasizing its potential to overcome classical limitations such as low computational efficiency and data scarcity through enhanced optimization and execution speed. [34] conducted a comprehensive review of 28 QML studies published between 2018 and 2024, reporting the prevalent use of quantum support vector machines (QSVMs), quantum convolutional neural networks (QCNNs), and hybrid quantum-classical models in applications including brain tumor and COVID-19 image classification. They also highlighted ongoing challenges in data encoding and the limitations of current quantum hardware. [35] proposed a 2D hybrid QFT-based quantum image processing method for image analysis and synthesis, demonstrating the efficacy of Fourier-transform operations in quantum pipelines. Additionally, [36] reviewed the application of quantum algorithms in medical image processing, particularly in tasks such as feature extraction, segmentation, and classification.

[37] investigated quantum neural network techniques for medical image classification using retinal fundus and chest X-ray images, highlighting both the potential advantages and the current hardware limitations of quantum methods.

On the generative front, [38] introduced Quantum Image Generative Learning (QIGL) for synthesizing high-resolution medical images. Their model used variational circuits and Wasserstein loss to produce diagnostically relevant synthetic data, aiding model generalization under limited data settings.

[39] presents a comparative analysis between classical Convolutional Neural Networks (CNNs) and a novel Quantum Convolutional Neural Network (QCNN) tailored for image classification tasks, particularly focusing on COVID-19 chest X-ray images. The QCNN demonstrates superior performance in recognition accuracy and processing speed when trained on the COVIDx-CXR-3 dataset, showcasing the potential of quantum computing to enhance image classification.

[40] further demonstrated the utility of hybrid quantum convolutional neural networks (HQCNNs) in pre-training MRI datasets, such as brain tumors, indicating the adaptability of these models to different medical imaging challenges.

While the above approaches demonstrate promising capabilities, there remains a clear research gap:

- Most QNN or QCNN models target binary classification and are trained on synthetic or grayscale datasets.
- Existing hybrid architectures lack attention mechanisms, hierarchical encoding, and superpositional entanglement required for structured medical images.
- No prior work, to the best of our knowledge, integrates cyclic U3 gate encoding, superpositional entanglement, and Fourier-based quantum attention within a unified model evaluated on diverse and noisy clinical datasets.

These findings reinforce the motivation for developing a robust and generalizable HQCNN architecture, one that integrates Fourier attention, cyclic U3 encoding, and entanglement in a principled manner to advance the state of quantum-enhanced image classification.

We propose a novel Hybrid Quantum-Classical Convolutional Neural Network (HQCNN) that incorporates:

- Quantum angle embedding with cyclic U3 rotation gates,
- A superpositional entanglement layer,
- A Quantum Fourier-inspired Attention (QAF) mechanism,
- Measuring via Pauli-Z expectation and classical dense layers.

We evaluated our HQCNN on six MedMNIST collections, covering both binary and multiclass tasks. Our extensive ablation study and comparative evaluation demonstrate the robustness and superiority of the proposed HQCNN over classical CNNs, ResNet, MedViT, and baseline QNNs, especially in noisy and imbalanced scenarios.

3 Methodology

In recent research, deep learning, particularly convolutional neural networks (CNNs), has demonstrated exceptional capabilities in feature extraction from medical images, enabling accurate identification of anatomical structures and disease-related patterns [1, 2]. Motivated by these advances, hybrid quantum-classical neural networks have emerged as promising alternatives, leveraging the non-classical expressivity of quantum circuits for learning complex patterns in low-dimensional feature spaces [22, 41].

To tackle the challenges of low-resolution medical image datasets, we propose HQCNN, a hybrid quantum-classical neural network architecture that leverages quantum encoding and entanglement to enhance class separability to classify medical images by combining classical preprocessing and quantum-enhanced feature learning. The model integrates classical data encoding with variational quantum transformations, allowing efficient representation and entanglement-based modeling of spatial and spectral patterns present in medical images. The overall architecture of HQCNN, illustrated in Figure 1, is structured into three primary stages: (1) a classical convolutional backbone, (2) a variational quantum circuit embedded within the feature processing pipeline, and (3) fully connected layers for final classification.

3.1 Classical Convolutional Backbone

In the classical stage, we employ a five-layer convolutional backbone to progressively extract hierarchical features from input medical images. Each layer is composed of convolutional operations followed by batch normalization and ReLU activation, with max pooling applied selectively to reduce spatial dimensions while preserving essential diagnostic information.

- **Layers 1–2:** Utilize 16 filters with 3×3 kernels, batch normalization, and ReLU activation to capture low-level features such as edges, contours, and gradients. Layer 2 incorporates max pooling to downsample spatial resolution.
- **Layers 3–4:** Expand to 64 filters with 3×3 kernels to extract mid-level patterns including textures, shapes, and cellular structures.
- **Layer 5:** Maintains 64 filters with 3×3 kernels, includes padding, and applies max pooling to encode high-level semantic features such as organ boundaries, lesion regions, and other diagnostically relevant structures.

This feature extraction design ensures that only the most salient and compressed representations are passed to the quantum circuit, enabling efficient quantum encoding and entanglement-based learning within the constrained qubit space.

3.2 Variational Quantum Circuit Design

The Variational Quantum Circuit (VQC) within the HQCNN architecture serves as the quantum processing core, transforming classically extracted features of `fc1` into expressive quantum representations. As illustrated in Figure2, the VQC is composed of several modular components, including Quantum State Encoding, Superpositional Entanglement, and the Quantum Attention-Fourier (QAF) Layer. Each module is specifically designed to enhance feature interaction, hierarchical attention modeling, and class separability within the quantum Hilbert space. The following subsections detail the structure and function of each component.

3.2.1 Quantum State Encoding Layer

The Quantum State Encoding Layer in our HQCNN model maps classical image features into the quantum Hilbert space using two key components: angle embedding and parameterized U3 rotations with cyclic wire mapping. This enables efficient data representation within a quantum circuit, improving expressivity while reducing model complexity.

(A) Angle Embedding into Quantum State

Angle embedding is a widely adopted method in variational quantum circuits (VQCs) for converting classical data into quantum states. In our implementation, we utilize the RY gate to encode each element of a normalized input vector $\mathbf{x} = [x_0, x_1, ..., x_{n-1}] \in \mathbf{R}^n$ onto an n-qubit quantum register:

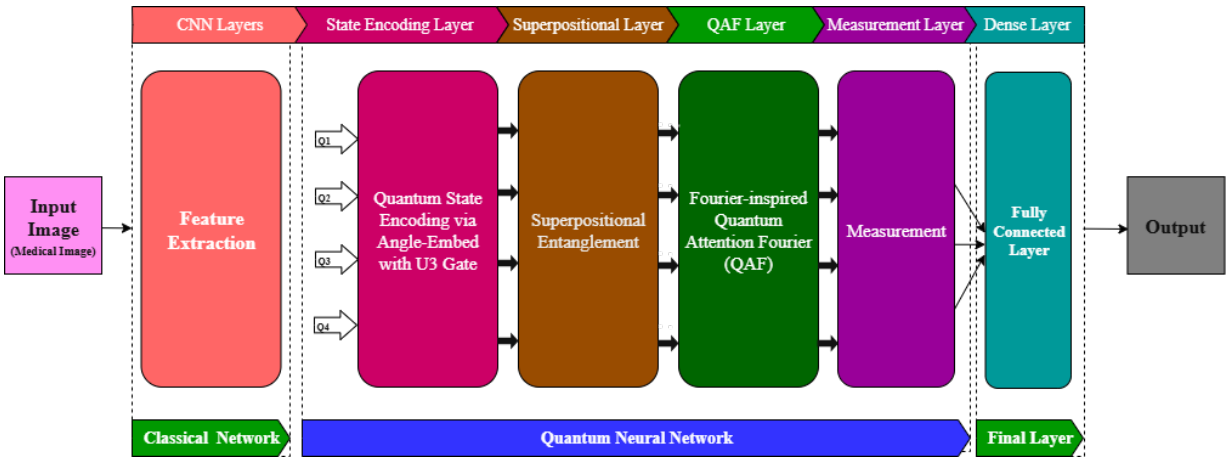

Figure 1: The proposed Hybrid Quantum-Classical Neural Network (HQCNN) architecture processes input medical images through a classical convolutional backbone for spatial feature extraction. These features are then passed to a 4-qubit variational quantum circuit comprising quantum state encoding, superpositional entanglement, and a Fourier-inspired Quantum Attention Fourier (QAF) layer. The quantum features are measured using Pauli observables and subsequently fed into fully connected layers for final classification.

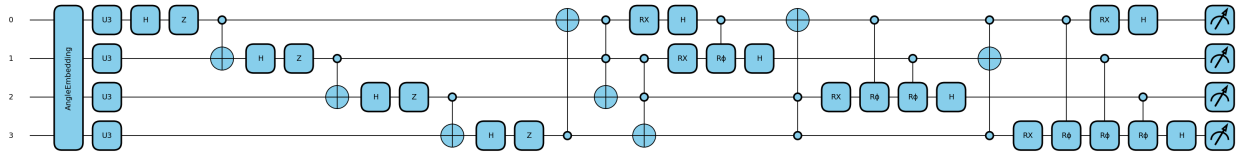

Figure 2: Illustration of the 4-qubit quantum circuit architecture used within HQCNN, highlighting key components such as angle embedding, cyclic U3 rotations, entanglement via CNOT gates, and the QAF layer

$$|\psi_0\rangle = |0\rangle^{\otimes n} \xrightarrow{\text{AngleEmbedding}} |\psi_{\text{embed}}\rangle = \bigotimes_{i=0}^{n-1} RY(x_i)\,|0\rangle \tag{1}$$

Each x_i element encodes a rotation on the i-th qubit using:

$$RY(x_i) = \begin{bmatrix} \cos\left(\frac{x_i}{2}\right) & -\sin\left(\frac{x_i}{2}\right) \\ \sin\left(\frac{x_i}{2}\right) & \cos\left(\frac{x_i}{2}\right) \end{bmatrix} \tag{2}$$

This operation initializes the quantum state in a data-dependent configuration, encoding classical information as quantum amplitudes for downstream processing.

(B) Parameterized U_3 Encoding with Cyclic Wire Mapping

The U3 gates offer complete controllability over single-qubit states, enabling better feature encoding for complex-valued medical images. To enrich the expressiveness of the quantum encoding, we apply parameterized U_3 gates following the angle embedding. The U_3 gate is the most general single-qubit unitary operator and is defined as:

$$U_3(\theta, \phi, \lambda) = \begin{bmatrix} \cos(\theta/2) & -e^{i\lambda}\sin(\theta/2) \\ e^{i\phi}\sin(\theta/2) & e^{i(\phi+\lambda)}\cos(\theta/2) \end{bmatrix} \tag{3}$$

It can be decomposed into standard rotation gates as follows:

$$U_3(\theta, \phi, \lambda) = RZ(\phi) \cdot RY(\theta) \cdot RZ(\lambda) \tag{4}$$

Here:

- θ modulates the amplitude via RY rotation,
- ϕ and λ encode global and relative phase shifts via RZ rotations.

To further encourage feature interaction across qubits, we employ a cyclic wire mapping strategy. Rather than applying the parameter set $(\theta_i, \phi_i, \lambda_i)$ to qubit q_i, we apply it to qubit $q_{(i+1) \bmod n}$, enabling shift-invariant transformations and promoting cross-qubit entanglement:

$$U_3(\theta_i, \phi_i, \lambda_i) \rightarrow q_{(i+1) \bmod n} \tag{5}$$

The full quantum state after angle embedding and U_3 transformations becomes:

$$|\psi_{\text{encoded}}\rangle = \prod_{i=0}^{n-1} U_3(\theta_i, \phi_i, \lambda_i)_{q_{(i+1) \bmod n}} \bigotimes_{i=0}^{n-1} RY(x_i) |0\rangle \tag{6}$$

This encoding captures local information from the classical input while preparing the quantum system for global correlation modeling through subsequent entanglement operations. Its ability to represent spatially distributed patterns is especially important for medical imaging tasks involving subtle, multi-region anomalies, e.g., lesions in BreastMNIST.

3.2.2 Superpositional Entanglement Layer

The Superpositional Entanglement Layer in our HQCNN architecture introduces both quantum superposition and entanglement to enrich the representational capacity of encoded quantum states. Following the quantum state encoding stage, each qubit is first transformed into a superposed state using Hadamard gates, then modified via Pauli-Z operations for phase control, and finally entangled through a cyclic sequence of CNOT gates. This layered transformation enables the quantum circuit to model both local and global feature dependencies, essential for tasks like medical image classification, where diagnostic cues may span multiple spatial regions.

(A) Applying Hadamard Gates (Superposition)

Each qubit q_i is placed into a superposition via the Hadamard gate:

$$H |0\rangle = \frac{1}{\sqrt{2}}(|0\rangle + |1\rangle), \quad H |1\rangle = \frac{1}{\sqrt{2}}(|0\rangle - |1\rangle)$$

Applying Hadamard gates across all qubits produces:

$$|\psi_1\rangle = \bigotimes_{i=0}^{n-1} H_i \ |\psi_{\text{encoded}}\rangle \tag{7}$$

This step enables the circuit to explore multiple basis states simultaneously, allowing for rich and distributed representations.

(B) Applying Pauli-Z Gates (Phase Encoding)

Next, each qubit undergoes a Pauli-Z operation, which introduces a phase flip to the $|1\rangle$ state:

$$Z |0\rangle = |0\rangle, \quad Z |1\rangle = -|1\rangle, \quad Z = \begin{bmatrix} 1 & 0 \\ 0 & -1 \end{bmatrix}$$

The state becomes:

$$|\psi_2\rangle = \bigotimes_{i=0}^{n-1} Z_i H_i \ |\psi_{\text{encoded}}\rangle \tag{8}$$

This phase modulation is particularly useful for capturing contrast differences and textural features, which are critical in modalities like histopathology and grayscale X-ray imaging.

(C) Applying CNOT Gates (Cyclic Entanglement)

To capture global feature interactions, we apply cyclic CNOT entanglement, where each qubit is entangled with its successor (modulo n):

$$\text{CNOT}(q_i, q_{(i+1) \bmod n}), \quad \forall i \in \{0, 1, \ldots, n-1\} \tag{9}$$

For a 4-qubit circuit, the entanglement sequence is:

$$\text{CNOT}(q_0, q_1), \quad \text{CNOT}(q_1, q_2), \quad \text{CNOT}(q_2, q_3), \quad \text{CNOT}(q_3, q_0)$$

This cyclic entanglement ensures bidirectional correlation and preserves permutation invariance across the register.

The resulting entangled quantum state is:

$$|\psi_{\text{entangled}}\rangle = \left(\prod_{i=0}^{n-1} \text{CNOT}(q_i, q_{(i+1) \bmod n}) \cdot Z_i H_i \right) |\psi_{\text{encoded}}\rangle \tag{10}$$

This state encodes rich amplitude and phase correlations, making it highly expressive for downstream layers such as quantum attention and measurement. The joint modeling of local and global dependencies makes the layer particularly powerful for structured medical image analysis, where abnormal features are often spatially distributed.

3.2.3 Hierarchical Quantum Attention-Fourier (QAF) Layer

In classical deep learning, attention mechanisms [42] and spectral transforms such as the Discrete Fourier Transform (DFT) [43] have proven highly effective in modeling global dependencies, long-range interactions, and hierarchical abstraction across input data. These techniques are widely applied in domains such as natural language processing and computer vision, where global context plays a vital role.

Inspired by these classical ideas, we propose the Quantum Attention-Fourier (QAF) Layer, a novel quantum circuit component that integrates quantum attention modulation, Fourier-inspired phase encoding, and basis transformation. This layer enables our HQCNN model to encode both local entanglement and global spectral structure directly into quantum states, thereby capturing rich spatial and frequency-based patterns from medical images. The design builds upon emerging quantum attention frameworks [44], extending their utility to hierarchical spatial analysis. The layer design architecture is explained in the subsequent sections.

Each qubit $q_i \in \{0, 1, \ldots, n-1\}$ undergoes a three-stage transformation sequence:

(A) Attention via Toffoli and RX Gates

We begin with a controlled Toffoli gate to entangle three neighboring qubits, modeling a local attention mechanism. The Toffoli gate activates a NOT operation on q_{i+2} conditioned on both q_i and q_{i+1} being in state $|1\rangle$:

$$\text{Toffoli}(q_i, q_{(i+1) \bmod n}, q_{(i+2) \bmod n}) = |11\rangle\langle 11|_{i,i+1} \otimes X_{i+2} + \Big(I - |11\rangle\langle 11|_{i,i+1}\Big) \otimes I_{i+2} \tag{11}$$

This is followed by a deterministic rotation:

$$R_X^{(i)}\left(\frac{\pi}{2}\right) = \exp\left(-i\frac{\pi}{4}X\right) = \frac{1}{\sqrt{2}}(I - iX) \tag{12}$$

Together, this block simulates attention-weighted activation across qubits and facilitates coherent superposition, enhancing representational capacity.

(B) Fourier-Inspired Phase Encoding

To model global dependencies, each qubit q_i interacts with all lower-index qubits q_j $(j < i)$ via controlled phase gates with exponentially decaying weights:

$$\text{CPhase}_{j,i}\left(\frac{\pi}{2^{i-j}}\right) = |0\rangle\langle 0|_j \otimes I_i + |1\rangle\langle 1|_j \otimes R_Z^{(i)}\left(\frac{\pi}{2^{i-j}}\right) \tag{13}$$

where the phase shift is implemented by:

$$R_Z(\phi) = e^{-i\phi/2}|0\rangle\langle 0| + e^{i\phi/2}|1\rangle\langle 1| \tag{14}$$

This phase modulation mimics Fourier basis construction, enabling frequency-sensitive relationships to be embedded directly into the quantum state.

(C) Basis Transformation via Hadamard Gate

A Hadamard gate is then applied to project accumulated phase information into an observable measurement basis:

$$H = \frac{1}{\sqrt{2}}\begin{bmatrix} 1 & 1 \\ 1 & -1 \end{bmatrix}.$$

$$H|0\rangle = \frac{1}{\sqrt{2}}(|0\rangle + |1\rangle), \quad H|1\rangle = \frac{1}{\sqrt{2}}(|0\rangle - |1\rangle).$$

This final transformation transforms relative phases into amplitude-based features suitable for quantum measurement and classification.

The composite operation on qubit q_i is given by:

$$U_{\text{QAF}}(i) = H(q_i) \cdot \left(\prod_{j=0}^{i-1} \text{CPhase}_{j,i}\left(\frac{\pi}{2^{i-j}}\right)\right) \cdot R_X^{(i)}\left(\frac{\pi}{2}\right) \cdot \text{Toffoli}(q_i, q_{(i+1) \bmod n}, q_{(i+2) \bmod n}) \tag{15}$$

The full layer transformation over all n-qubits becomes:

$$U_{\text{QAF}} = \prod_{i=0}^{n-1} U_{\text{QAF}}(i) \tag{16}$$

$$|\psi'\rangle = U_{\text{QAF}}|\psi_{\text{entangled}}\rangle \tag{17}$$

This sequence enables the circuit to capture both entangled local interactions and global spectral structures within the quantum state space.

A high-level algorithm for implementing the Hierarchical Quantum Attention-Fourier (QAF) Layer in the PennyLane framework is presented below in Algorithm 1:

Final quantum state $|\psi'\rangle$ captures entangled attention, spectral phase dynamics, and hierarchical spatial information, enhancing the model's ability to interpret long-range structure in noisy, low-resolution medical images.

Algorithm 1 Hierarchical Quantum Attention-Fourier (QAF) Layer

Input: Quantum state $|\psi_{\text{entangled}}\rangle$ over n qubits; fixed rotation angle $\theta = \frac{\pi}{2}$
Output: Updated quantum state $|\psi'\rangle$ with entangled attention and spectral encoding

for $i = 0$ to $n-1$ **do**
    (1) Apply Quantum Attention (Toffoli + R_X) Block
    Apply Toffoli gate on qubits (q_i, $q_{(i+1)} \bmod n$, $q_{(i+2)} \bmod n$)
    Apply single-qubit rotation $R_X(\theta)$ to q_i

    (2) Encode Fourier-Inspired Spectral Phases
    for $j = 0$ to $i-1$ **do**
        Apply controlled-phase gate $\text{CPhase}\left(\frac{\pi}{2^{i-j}}\right)$ between q_j (control) and q_i (target)
    end for

    (3) Project into Measurement Basis
    Apply Hadamard gate H to q_i
end for

3.2.4 Measurement: Quantum State to Classical Feature Extraction

Quantum computations manipulate data encoded in quantum state vectors $|\psi\rangle$ within high-dimensional Hilbert spaces, evolving through unitary transformations. In the proposed HQCNN framework, the final quantum state encodes entangled, spectrally modulated, and hierarchically structured representations of the input medical image. This is achieved through the sequential application of four key quantum modules: *Angle Embedding*, *cyclic U3 encoding*, *Superpositional Entanglement*, and the *Quantum Attention-Fourier (QAF) Layer*.

The complete unitary evolution of the system yields the final quantum state:

$$|\psi_{\text{final}}\rangle = U_{\text{QAF}} \cdot U_{\text{SuperEntangle}} \cdot U_3 \cdot |\psi_{\text{embed}}\rangle \quad (18)$$

To translate this high-dimensional quantum state into a classical feature space suitable for downstream classification, we perform expectation value measurements on each qubit $q_i \in \{0, 1, \ldots, n-1\}$ over two complementary Pauli bases:

- **Pauli-Z (computational basis):** $f_i^{(Z)} = \langle\psi|Z_i|\psi\rangle$
- **Pauli-X (superposition basis):** $f_i^{(X)} = \langle\psi|X_i|\psi\rangle$

This hybrid measurement strategy enables the extraction of both localized activations (via Z) and distributed superpositional features (via X), capturing orthogonal perspectives on the encoded information. The resulting classical feature vector is given by:

$$\mathbf{f}_{\text{quantum}} = \left[f_0^{(Z)}, \ldots, f_{n-1}^{(Z)}, f_0^{(X)}, \ldots, f_{n-1}^{(X)}\right] \in \mathbf{R}^{2n}$$

By combining measurements across both eigenbases, the model gains access to rich representational cues—such as boundary sharpness, spatial symmetry, and textural intensity—critical for robust medical image classification.

3.3 Classical Fully Connected Layer

The quantum circuit in Fig. 2 returns $\mathbf{f}_{\text{quantum}}$, a vector of expectation values, which is passed to `fc2` to expand into a 128-dimensional latent representation. Finally, `fc3` produces class predictions. A softmax activation is applied for multi-class classification (e.g., PathMNIST or OrganAMNIST), while a sigmoid activation is used for binary classification tasks (e.g., BreastMNIST).

$$\mathbf{f}_{\text{quantum}} = [z_0, z_1, \ldots, z_{n-1}, x_0, x_1, \ldots, x_{n-1}]$$

This vector is passed through one or more fully connected (dense) layers to reduce the high-dimensional quantum state into a low-dimensional class representation suitable for classification.

Depending on the dataset and diagnostic requirement, the output layer uses an activation function aligned with the classification objective:

- **Binary classification** (e.g., BreastMNIST for benign vs. malignant):

$$\hat{y} = \frac{1}{1 + e^{-h}} \quad \text{(Sigmoid activation)}$$

- **Multi-class classification** (e.g., OrganAMNIST and PathMNIST):

$$\hat{y}_i = \frac{e^{h_i}}{\sum_{j=1}^{C} e^{h_j}}, \quad i = 1, \ldots, C \quad \text{(Softmax activation)}$$

These produce interpretable probabilistic outputs, allowing the model to assign class confidence for disease labels or anatomical types.

3.4 Training Pipeline

The HQCNN model is trained end-to-end using the training pipeline explained in Algorithm 2.

This hybrid pipeline ensures both classical and quantum parameters are optimized effectively, improving generalization in clinical applications.

Algorithm 2 Hybrid HQCNN Training Pipeline

```
Initialize parameters of classical CNN and quantum circuit.
for each epoch do
    for each mini-batch do
        Encode classical features into quantum states.
        Apply hybrid quantum layers (U3, entanglement, QAF).
        Measure the quantum outputs and pass them to the classifier.
        Compute loss and backpropagate (via parameter-shift rule for quantum).
    end for
    if Validation performance plateaued then
        Apply early stopping.
    end if
end for
return Optimized model
```

4 Results and Discussion

We describe the data preprocessing pipeline, which plays a crucial role in aligning classical image representations with the requirements of quantum circuits. This section presents the experimental results of the proposed HQCNN model for binary and multi-class medical image classification tasks. The performance is evaluated on six datasets from the MedMNIST v2 benchmark, a standardized suite of biomedical imaging tasks designed for lightweight supervised learning. Given the sensitivity of quantum circuits to input dimensionality and amplitude constraints, we carefully preprocess images via resizing, normalization, and dimension reduction to match the quantum register size. The processed inputs are encoded into quantum states using *AngleEmbedding* [45, 14], ensuring faithful translation of visual features into a quantum-compatible format suitable for variational learning.

4.1 Dataset Overview

We utilize six publicly available biomedical imaging datasets from the MedMNIST v2 benchmark [6] to individually evaluate the performance and generalization capability of our proposed Hybrid Quantum-Classical Neural Network (HQCNN). These datasets encompass multiple imaging modalities, including histopathology, CT, ultrasound, X-ray, microscopy, and Optical Coherence Tomography (OCT), and support both binary and multi-class classification tasks.

All datasets are preprocessed into 28×28 resolution and follow a standardized three-way split (training, validation, test), enabling reproducibility and fair comparison across tasks of varying complexity. The datasets employed in this study are summarized in Table 1.

All datasets used in this study (e.g., PathMNIST, OrganAMNIST, etc.) are publicly available from the MedMNIST2D repository. These datasets are anonymized and do not contain personally identifiable information. Therefore, no ethical approval was required.

4.2 Evaluation Metrics and Baselines

To comprehensively assess the performance, we adopt a diverse set of standard evaluation metrics alongside robust classical and hybrid baseline models of the proposed Hybrid Quantum-Classical Neural Network (HQCNN). This implies for quantitative benchmarking across binary and multi-class medical image classification tasks.

Evaluation Metrics

The following set of metrics are used to evaluate the predictive performance of the model across different datasets:

- **Accuracy (ACC)**
  Measures the overall proportion of correctly classified samples:

$$\text{Accuracy} = \frac{TP + TN}{TP + TN + FP + FN}$$

  Where:

  - TP = True Positives
  - TN = True Negatives
  - FP = False Positives
  - FN = False Negatives

- **Area Under the ROC Curve (AUC)**
  AUC reflects the model's ability to distinguish between classes across all decision

Table 1: Summary of MedMNIST v2 datasets used in this study. Each dataset differs in modality, task with class count, and diagnostic focus.

Dataset	Modality	Samples	Train / Val / Test	Task(Classes)	Clinical Focus
PathMNIST	Histopathology (RGB)	107,180	89,996 / 10,004 / 7,180	Multi-class (9)	Colon tissue classification
OCTMNIST	OCT (grayscale)	109,309	97,477 / 10,832 / 1,000	Multi-class (4)	Retinal disease detection
PneumoniaMNIST	X-ray (grayscale)	5,856	4,708 / 524 / 624	Binary (2)	Pediatric pneumonia diagnosis
BreastMNIST	Ultrasound (grayscale)	780	546 / 78 / 156	Binary (2)	Breast tumor classification
BloodMNIST	Microscopy (RGB)	17,092	11,959 / 1,712 / 3,421	Multi-class (8)	Blood cell morphology analysis
OrganAMNIST	CT (grayscale)	58,830	34,561 / 6,491 / 17,778	Multi-class (11)	Abdominal organ classification

thresholds. It is especially useful in imbalanced datasets, providing a threshold-independent performance measure.

- **Precision**
  The proportion of true positive predictions among all predicted positives:

$$\text{Precision} = \frac{TP}{TP + FP}$$

- **Recall (Sensitivity)**
  The proportion of true positive predictions among all actual positives:

$$\text{Recall} = \frac{TP}{TP + FN}$$

All metrics are computed on the test set using standard MedMNIST splits and reported as macro-averaged values for multi-class tasks. To benchmark the HQCNN, we compare its performance against a set of classical and quantum baselines. These include:

- ResNet-18 and ResNet-50: Deep residual networks known for their strong performance on medical imaging tasks [15], evaluated at both 28×28 and 224×224 resolutions.
- MedViT: A hybrid convolutional-Transformer model designed for lightweight medical image classification, as introduced in the MedMNIST leaderboard [17].
- AutoKeras (Google AutoML Vision): A state-of-the-art neural architecture search framework that automatically selects optimal models for image classification [46].
- QNN: A MedMNIST benchmark using a 127-qubit IBM quantum computer, demonstrating the feasibility of pure QNNs with hardware-efficient circuits and error mitigation[19].

All baseline models are trained and evaluated on the same MedMNIST v2 dataset as our HQCNN model, using the standard train/val/test splits and metrics (Accuracy, AUC). We ensure fair comparisons by keeping data preprocessing and training settings consistent across experiments.

This comparative setup enables an objective analysis of how quantum circuit depth, entanglement structure, and hybrid attention mechanisms impact classification accuracy and robustness, particularly for small-scale medical image datasets with limited features and varying complexity. Comparative results are reported against classical baselines, including a standard ResNet-18, ResNet-50, MedViT, Google AutoML Vision, and pure Quantum Neural Network (QNN).

4.3 Quantitative Results

We evaluate the model using four standard performance metrics: *Accuracy (ACC)*, *Area Under the Receiver Operating Characteristic Curve (AUC)*, *Precision*, and *Recall*. Table 2 summarizes the HQCNN results across both binary and multi-class versions of each dataset.

To validate HQCNN's effectiveness, we compare its performance against five widely used baseline models: ResNet-18, ResNet-50, Google AutoML Vision, and pure Quantum Neural Network (QNN). These models are trained under identical data splits and quantum-compatible input resolution (28×28). Table 3 reports the comparative results across selected datasets.

Finally, Table 3 benchmarks HQCNN against published state-of-the-art classical models from the MedMNIST leaderboard. HQCNN shows competitive performance across several tasks, particularly in binary and multi-class classification.

These results demonstrate HQCNN's strong capability to learn discriminative features from

Table 2: Performance of HQCNN across binary and multi-class on MedMNIST datasets.

Dataset	Task Type	AUC (%)	Accuracy (%)	Precision (%)	Recall (%)
PathMNIST	Multi-class	99.59	93.40	93.00	93.00
PathMNIST (0 vs. 1)	Binary	100.00	99.91	100.00	100.00
OrganAMNIST	Multi-class	99.95	97.99	94.90	94.80
OrganAMNIST (0 vs. 1)	Binary	99.98	99.74	100.00	100.00
BloodMNIST	Multi-class	99.48	93.42	93.00	93.00
BloodMNIST (0 vs. 1)	Binary	99.10	99.19	99.00	99.00
OCTMNIST	Multi-class	97.20	91.57	91.00	92.00
OCTMNIST (0 vs. 1)	Binary	99.47	97.35	97.00	97.00
BreastMNIST	Binary	90.04	87.18	87.00	87.00
PneumoniaMNIST	Binary	98.89	96.16	96.00	96.00

Table 3: Comparison of the proposed HQCNN model with baseline models including ResNet-18, ResNet-50, MedViT, and Google AutoML Vision, as well as with a QNN implementation on real quantum hardware, evaluated on the MedMNIST benchmark datasets.

Method	PathMNIST		OrganAMNIST		BloodMNIST		OCTMNIST		BreastMNIST		PneumoniaMNIST	
	AUC	ACC	AUC	ACC	AUC	ACC	AUC	ACC	AUC	ACC	AUC	ACC
ResNet-18 (28)	0.983	0.907	0.997	0.935	0.998	0.958	0.943	0.743	0.901	0.863	0.944	0.854
ResNet-50 (28)	0.990	0.911	0.997	0.935	0.997	0.956	0.952	0.762	0.857	0.812	0.948	0.854
MedViT [17]	0.992	0.909	**0.997**	0.932	0.997	0.968	0.960	0.783	0.856	**0.891**	0.978	0.939
Google AutoML Vision	0.944	0.728	0.990	0.886	**0.998**	**0.966**	**0.963**	0.771	**0.919**	0.861	**0.991**	0.946
QNN [19]	0.784	0.3723	-	-	0.821	0.482	0.659	0.443	0.674	0.810	0.8197	0.8526
HQCNN (Ours)	**0.995**	**0.934**	**0.999**	**0.979**	**0.994**	**0.934**	**0.972**	**0.915**	**0.900**	**0.871**	**0.988**	**0.961**

low-resolution and clinically relevant image data. Particularly in binary classification tasks, the model benefits significantly from the entanglement-aware quantum attention and hybrid pooling strategies, outperforming both classical and quantum baselines.

4.4 Visual Analysis and Dataset-Specific Performance

To provide deeper insights into the training behavior and predictive robustness of the proposed HQCNN, we present dataset-specific performance visualizations. These include accuracy and loss curves over epochs, demonstrating convergence dynamics on representative MedMNIST datasets.

4.4.1 PathMNIST Dataset

The PathMNIST dataset contains histopathological images from colorectal cancer tissue. The HQCNN model attained a final test accuracy of 93.40% and 99.59% AUC in multi-class, and 99.91% accuracy with a perfect 100% AUC in binary classification task. It showed strong learning progression across epochs. The hybrid quantum layers effectively enhanced tissue differentiation, capturing complex local features in dense RGB-stained samples. Figure 3 illustrates the training and validation performance of HQCNN over 10 epochs, demonstrating rapid convergence and robust generalization.

4.4.2 OrganAMNIST Dataset

The OrganAMNIST dataset contains grayscale abdominal CT scans across 11 classes representing human organs. The proposed HQCNN model achieved a test accuracy of 97.99% with an AUC of 99.95% in multi-class and 99.74% accuracy with 99.98% AUC in binary classification. The hybrid quantum layers played a critical role in enhancing spatial encoding, particularly in cases where class boundaries are subtle due to overlapping anatomical structures, which contributes to improve in generalization performance throughout the training epochs. Figure 4 illustrates the training and validation performance of HQCNN over 10 epochs, demonstrating rapid convergence and robust generalization.

4.4.3 BloodMNIST Dataset

The BloodMNIST dataset contains microscopy images of blood cells that exhibit well-defined boundaries and high inter-class variance. The HQCNN model achieved an accuracy of 93.42% and an AUC of 99.48% in multi-class settings and 99.19% accuracy with 99.48% AUC in a binary classification task. The quantum layers of HQCNN effectively captured morphological variations between blood components, enabling near-perfect classification performance. Figure 5 illustrates the training and validation performance of HQCNN over 10 epochs.

4.4.4 OCTMNIST Dataset

The OCTMNIST dataset consists of retinal optical coherence tomography (OCT) images classified into four diagnostic categories. The HQCNN model achieved a test accuracy of 91.57% with 97.20% AUC in multi-class settings and 97.35% accuracy with 99.47% AUC in binary classification task. The quantum entanglement and attention layers effectively captured fine-grained texture and depth variations in the retinal images, leading to consistently improved performance across training epochs, as shown in Figure 6.

4.4.5 BreastMNIST Dataset

The BreastMNIST dataset contains 780 grayscale ultrasound images labeled for binary classification of benign vs. malignant lesions, in order to evaluate the HQCNN model's diagnostic performance under noise-prone and low-resolution grayscale conditions. The HQCNN model achieved a test accuracy of 87.18% and a validation AUC of 90.04%, converging stably within 10 epochs, as illustrated in Figure 7. The relatively lower performance is attributed to the limited sample size and noise inherent in low-resolution ultrasound images. Quantum feature encoding enhances to the model's sensitivity to subtle grayscale variations, which is critical for distinguishing tumor types with high intra-class similarity.

4.4.6 PneumoniaMNIST Dataset

The PneumoniaMNIST dataset pediatric chest X-ray images is classified as either normal or pneumonia based on binary class labels. The proposed HQCNN model achieved an AUC of 98.89% and a test accuracy of 96.16%, by leveraging on low-contrast grayscale images, which reflects strong diagnostic performance. The quantum feature extraction layers effectively captured subtle textural variations in lung regions, enhancing in class-imbalanced clinical conditions. Figure 8 illustrates the training and validation performance of HQCNN over 10 epochs.

These findings highlight the HQCNN model's capability and strong generalization across structurally diverse medical image modalities, from high-resolution histopathology to low-contrast grayscale X-rays. While classical convolutional layers preserved local morphological features, the integration of quantum components, such as entanglement, variational encoding, and the Quantum Attention-Fourier (QAF) layer, enhanced class separability and representation learning. This hybrid design led to smoother loss convergence, improved diagnostic accuracy, and outperformance of classical-only baselines, underscoring HQCNN's potential for existing clinical applications.

4.5 Ablation Study

To assess the contribution of individual components in our quantum circuit design, we perform an ablation study by selectively removing or modifying key layers in the Hybrid Quantum-Classical Convolutional Neural Network (HQCNN). This analysis highlights the role of each quantum operation in enhancing classification performance across both binary and multi-class tasks in biomedical imaging. The following configurations were evaluated:

- Full HQCNN (Ours): Complete architecture including AngleEmbedding, U3 rotation layer, Superpositional Entanglement, QAF (Toffoli + CPhase + Hadamard), and Fourier-inspired readout (RX + H).
- No QAF: Removes the hierarchical Quantum Attention based Fourier (Toffoli + CPhase + H) while retaining prior layers.
- No Superpositional Entanglement Layer: Eliminates Hadamard, Z, and cyclic CNOT gates to test the role of quantum correlations.

Table 4: Ablation studies across six MedMNIST datasets. Full HQCNN includes all quantum components.

Variant	PathMNIST		OrganAMNIST		BloodMNIST		OCTMNIST		BreastMNIST		PneumoniaMNIST	
	ACC	AUC	ACC	AUC	ACC	AUC	ACC	AUC	ACC	AUC	ACC	AUC
Full HQCNN (Ours)	**93.40**	**99.59**	**97.99**	**99.95**	**93.42**	**99.48**	**91.57**	**97.20**	**87.18**	**90.04**	**96.08**	**98.89**
No QAF	92.33	99.56	97.15	97.90	92.63	99.45	89.51	94.55	83.33	86.97	95.56	98.62
No Superpositional Entanglement	91.73	99.44	97.04	99.91	92.60	99.32	86.59	88.12	81.41	83.64	95.73	98.83
U3 → RX only	92.79	99.55	96.58	99.87	89.85	99.00	88.27	91.04	85.90	87.28	95.31	98.63

- U3 → RX only: Replaces expressive U3 gates with simpler RX rotations to analyze parametrization sensitivity.

Key Observations:

- Removing the QAF block (Toffoli + CPhase + H) caused the most significant performance drop, confirming its role in enhancing hierarchical feature encoding via multi-controlled phase interactions.
- The absence of entanglement (Hadamard + Pauli-Z + cyclic CNOT) led to lower accuracy across all datasets, highlighting the need for quantum correlations among qubits.
- Simplifying the U3 gates to only RX reduces the circuit's expressivity, impacting classification performance—especially on high-variance datasets like OCTMNIST and BreastMNIST.

These results validate the hierarchical design of the HQCNN circuit, where each quantum component contributes uniquely to extracting expressive, discriminative features from low-resolution biomedical images.

5 Conclusion

In recent years, the use of convolutional neural networks (CNNs) has substantially improved medical image analysis by enabling accurate extraction of anatomical and pathological features. But they often struggle with complex and low-resolution medical data. By leveraging quantum principles, hybrid quantum-classical models address these challenges and offer enhanced robustness and efficiency in capturing global patterns within compact feature spaces. In this study, we proposed a novel Hybrid Quantum-Classical Neural Network (HQCNN) for medical image classification, combining a five-layer classical convolutional backbone with a four-qubit variational quantum circuit. The quantum module incorporates quantum state encoding, superpositional entanglement, and a Fourier-inspired Quantum Attention Layer (QAF), enabling enhanced global feature representation and improved discriminative power. The HQCNN was evaluated on six benchmark datasets from the MedMNIST v2 suite, demonstrating consistent superiority over classical and quantum baseline models in both binary and multi-class classification tasks. Notably, it achieved 99.91% accuracy and 100.00% AUC on the PathMNIST binary classification task and exhibited strong robustness on noise-prone datasets such as BreastMNIST, attaining 87.18% accuracy. These results validate the efficacy of quantum-enhanced learning for complex medical image analysis while maintaining parameter efficiency. Despite these promising outcomes, a current limitation is the reliance on simulators due to hardware constraints. Moreover, the high computational overhead of quantum simulation poses a challenge for real-time clinical integration. These limitations highlight the gap between theoretical quantum models and their practical deployment in clinical settings. Future work will explore scaling the HQCNN to handle 3D volumetric medical data, such as CT or MRI scans, and investigate deeper quantum circuit designs optimized for execution on real quantum hardware. Overall, this work lays a foundational step toward quantum-integrated diagnostic intelligence, offering a promising direction for next-generation biomedical imaging applications.

Acknowledgments

The authors acknowledge the maintainers of the MedMNIST v2 dataset for providing standardized biomedical image benchmarks that supported this research. The authors are also grateful to their colleagues and the anonymous reviewers for their constructive feedback, which has helped improve the quality of this manuscript.

References

[1] Geert Litjens, Thijs Kooi, Babak Ehteshami Bejnordi, Arnaud Arindra Adiyoso Setio, Francesco Ciompi, Mohsen Ghafoorian, Jeroen Awm Van Der Laak, Bram Van Ginneken, and Clara I Sánchez. "A survey on deep learning in medical image analysis". Medical image analysis **42**, 60–88 (2017).

[2] Andre Esteva, Brett Kuprel, Roberto A Novoa, Justin Ko, Susan M Swetter, Helen M Blau, and Sebastian Thrun. "Dermatologist-level classification of skin cancer with deep neural networks". nature **542**, 115–118 (2017).

[3] Pranav Rajpurkar, Jeremy Irvin, Kaylie Zhu, Brandon Yang, Hershel Mehta, Tony Duan, Daisy Ding, Aarti Bagul, Curtis Langlotz, Katie Shpanskaya, Matthew P. Lungren, and Andrew Y. Ng. "Chexnet: Radiologist-level pneumonia detection on chest x-rays with deep learning" (2017). arXiv:1711.05225.

[4] Olaf Ronneberger, Philipp Fischer, and Thomas Brox. "U-net: Convolutional networks for biomedical image segmentation". In Medical Image Computing and Computer-Assisted Intervention – MICCAI 2015. Pages 234–241. Springer International Publishing (2015).

[5] Andrew G. Howard, Menglong Zhu, Bo Chen, Dmitry Kalenichenko, Weijun Wang, Tobias Weyand, Marco Andreetto, and Hartwig Adam. "Mobilenets: Efficient convolutional neural networks for mobile vision applications" (2017). arXiv:1704.04861.

[6] Jiancheng Yang, Rui Shi, Donglai Wei, Zequan Liu, Lin Zhao, Bilian Ke, Hanspeter Pfister, and Bingbing Ni. "Medmnist v2-a large-scale lightweight benchmark for 2d and 3d biomedical image classification". Scientific Data **10**, 41 (2023).

[7] Benoit Frenay and Michel Verleysen. "Classification in the presence of label noise: A survey". IEEE Transactions on Neural Networks and Learning Systems **25**, 845–869 (2014).

[8] Curtis Northcutt, Lu Jiang, and Isaac Chuang. "Confident learning: Estimating uncertainty in dataset labels". J. Artif. Int. Res. **70**, 1373–1411 (2021).

[9] Klaus-Robert Müller Wojciech Samek, Thomas Wiegand. "Explainable artificial intelligence: Understanding, visualizing and interpreting deep learning models" (2017).

[10] Cynthia Rudin. "Stop explaining black box machine learning models for high stakes decisions and use interpretable models instead". Nature Machine Intelligence **1**, 206–215 (2019).

[11] Iris Cong, Soonwon Choi, and Mikhail D. Lukin. "Quantum convolutional neural networks". Nature Physics **15**, 1273–1278 (2019).

[12] Adrián Pérez-Salinas, Alba Cervera-Lierta, Elies Gil-Fuster, and José I Latorre. "Data re-uploading for a universal quantum classifier". Quantum **4**, 226 (2020).

[13] Fan Fan, Yilei Shi, Tobias Guggemos, and Xiao Xiang Zhu. "Hybrid quantum-classical convolutional neural network model for image classification". IEEE Transactions on Neural Networks and Learning Systems **35**, 18145–18159 (2024).

[14] PennyLane Development Team. "Pennylane documentation: Angleembedding" (2023). `https://docs.pennylane.ai/`.

[15] Kaiming He, Xiangyu Zhang, Shaoqing Ren, and Jian Sun. "Deep residual learning for image recognition". In 2016 IEEE Conference on Computer Vision and Pattern Recognition (CVPR). Pages 770–778. (2016).

[16] Gao Huang, Zhuang Liu, Laurens Van Der Maaten, and Kilian Q. Weinberger. "Densely connected convolutional networks". In 2017 IEEE Conference on Computer Vision and Pattern Recognition (CVPR). Pages 2261–2269. (2017).

[17] Yan Liu. "Medical image classification based on transformer model and ordinal loss". In Proceedings of the 16th International Conference on Health Informatics (HEALTHINF). SCITEPRESS - Science and Technology Publications (2024).

[18] Haifeng Jin, Qingquan Song, and Xia Hu. "Auto-keras: An efficient neural architecture search system". In Proceedings of the 25th ACM SIGKDD International Conference on Knowledge Discovery & Data Mining. Page 1946–1956. KDD '19New York,

NY, USA (2019). Association for Computing Machinery.

[19] Gurinder Singh, Hongni Jin, and Kenneth M. Merz. "Benchmarking medmnist dataset on real quantum hardware" (2025). arXiv:2502.13056.

[20] Kinshuk Sengupta and Praveen Ranjan Srivastava. "Quantum algorithm for quicker clinical prognostic analysis: An application and experimental study using ct scan images of covid-19 patients". BMC Medical Informatics and Decision Making (2021).

[21] Alessandro Sebastianelli, Daniela Alessandra Zaidenberg, Dario Spiller, Bertrand Le Saux, and Silvia Liberata Ullo. "On circuit-based hybrid quantum neural networks for remote sensing imagery classification". IEEE Journal of Selected Topics in Applied Earth Observations and Remote Sensing **15**, 565–580 (2022).

[22] Maria Schuld and Nathan Killoran. "Quantum machine learning in feature hilbert spaces". Phys. Rev. Lett. **122**, 040504 (2019).

[23] Maxwell Henderson, Samriddhi Shakya, Shashindra Pradhan, and Tristan Cook. "Quanvolutional neural networks: Powering image recognition with quantum circuits". Quantum Machine Intelligence **2**, 2 (2020).

[24] Denis Bokhan, Alena S. Mastiukova, Aleksey S. Boev, Dmitrii N. Trubnikov, and Aleksey K. Fedorov. "Corrigendum: Multiclass classification using quantum convolutional neural networks with hybrid quantum-classical learning". Frontiers in Physics **10**, 1112211 (2023).

[25] Andrea Mari, Thomas R. Bromley, Josh Izaac, Maria Schuld, and Nathan Killoran. "Transfer learning in hybrid classical-quantum neural networks". Quantum **4**, 340 (2020). arXiv:1912.08278.

[26] Yangyang Li, Zhengya Qia, Yuelin Lia, Haorui Yanga, Ronghua Shanga, and Licheng Jiaoa. "A distributed hybrid quantum convolutional neural network for medical image classification" (2025). arXiv:2501.06225.

[27] Essam H Houssein, Zainab Abohashima, Mohamed Elhoseny, and Waleed M Mohamed. "Hybrid quantum-classical convolutional neural network model for covid-19 prediction using chest x-ray images". Journal of Computational Design and Engineering **9**, 343–363 (2022). arXiv:https://academic.oup.com/jcde/article-pdf/9/2/343/42616958/qwac003.pdf.

[28] Arsenii Senokosov, Alexandr Sedykh, Asel Sagingalieva, Basil Kyriacou, and Alexey Melnikov. "Quantum machine learning for image classification" (2024).

[29] Naim Ajlouni, Adem Özyavaş, Mustafa Takaoğlu, Faruk Takaoğlu, and Firas Ajlouni. "Medical image diagnosis based on adaptive hybrid quantum cnn". BMC Medical Imaging **23**, 126 (2023).

[30] Muhammad Al-Zafar Khan, Abdullah Al Omar Galib, Nouhaila Innan, and Mohamed Bennai. "Brain tumor diagnosis using hybrid quantum convolutional neural networks" (2025).

[31] Jonas Landman, Natansh Mathur, Yun Yvonna Li, Martin Strahm, Skander Kazdaghli, Anupam Prakash, and Iordanis Kerenidis. "Quantum Methods for Neural Networks and Application to Medical Image Classification". Quantum **6**, 881 (2022).

[32] Guangxi Li, Ruilin Ye, Xuanqiang Zhao, and Xin Wang. "Concentration of data encoding in parameterized quantum circuits". In Proceedings of the 36th International Conference on Neural Information Processing Systems. NIPS '22Red Hook, NY, USA (2022). Curran Associates Inc.

[33] Lin Wei, Haowen Liu, Jing Xu, Lei Shi, Zheng Shan, Bo Zhao, and Yufei Gao. "Quantum machine learning in medical image analysis: A survey". Neurocomputing **525**, 42–53 (2023).

[34] Eman A. Radhi, Mohammed Y. Kamil, and Mazin Abed Mohammed. "Quantum machine and deep learning for medical image classification: A systematic review of trends, methodologies, and future directions". Iraqi Journal for Computer Science and Mathematics **6**, Article 9 (2025).

[35] Tanay Kamlesh Patel, Danielle Knutson, Glen Uehara, Frank Marfai, Carly Jazwin, Jean Larson, and Andreas Spanias. "Image analysis-synthesis using the quantum fourier transform". In 2025 IEEE International Symposium on Circuits and Systems (ISCAS). Pages 1–5. (2025).

[36] Fei Yan, Hesheng Huang, Witold Pedrycz, and Kaoru Hirota. "Review of medical image processing using quantum-enabled algorithms". Artificial Intelligence Review **57**, 300 (2024).

[37] Natansh Mathur, Jonas Landman, Yun Yvonna Li, Martin Strahm, Skander Kazdaghli, Anupam Prakash, and Iordanis Kerenidis. "Medical image classification via quantum neural networks" (2021). arXiv:2109.01831.

[38] Amena Khatun, Kübra Yeter Aydeniz, Yaakov S Weinstein, and Muhammad Usman. "Quantum generative learning for high-resolution medical image generation". Machine Learning: Science and Technology **6**, 025032 (2025).

[39] Mohammed Yousif, Belal Al-Khateeb, and Begonya Garcia-Zapirain. "A new quantum circuits of quantum convolutional neural network for x-ray images classification". IEEE Access **12**, 65660–65671 (2024).

[40] Yumin Dong, Xuanxuan Che, Yanying Fu, Hengrui Liu, Yang Zhang, and Yong Tu. "Classification of knee osteoarthritis based on quantum-to-classical transfer learning". Frontiers in Physics**11** (2023).

[41] K. Mitarai, M. Negoro, M. Kitagawa, and K. Fujii. "Quantum circuit learning". Phys. Rev. A **98**, 032309 (2018).

[42] Ashish Vaswani, Noam Shazeer, Niki Parmar, Jakob Uszkoreit, Llion Jones, Aidan N Gomez, Łukasz Kaiser, and Illia Polosukhin. "Attention is all you need". Advances in neural information processing systems**30** (2017).

[43] ROren Rippel, Jasper Snoek, and Ryan P. Adams. "Spectral representations for convolutional neural networks". Advances in Neural Information Processing Systems**28** (2015). arXiv:1506.03767.

[44] Fu Chen, Qinglin Zhao, Li Feng, Chuangtao Chen, Yangbin Lin, and Jianhong Lin. "Quantum mixed-state self-attention network". Neural Networks **185**, 107123 (2025).

[45] Maria Schuld and Francesco Petruccione. "Machine learning with quantum computers". Pages XIV, 312. Quantum Science and Technology. Springer Cham. (2021). 2 edition.

[46] Haifeng Jin, Qingquan Song, and Xia Hu. "Auto-keras: An efficient neural architecture search system". In Proceedings of the 25th ACM SIGKDD International Conference on Knowledge Discovery & Data Mining. Page 1946–1956. KDD '19New York, NY, USA (2019). Association for Computing Machinery.

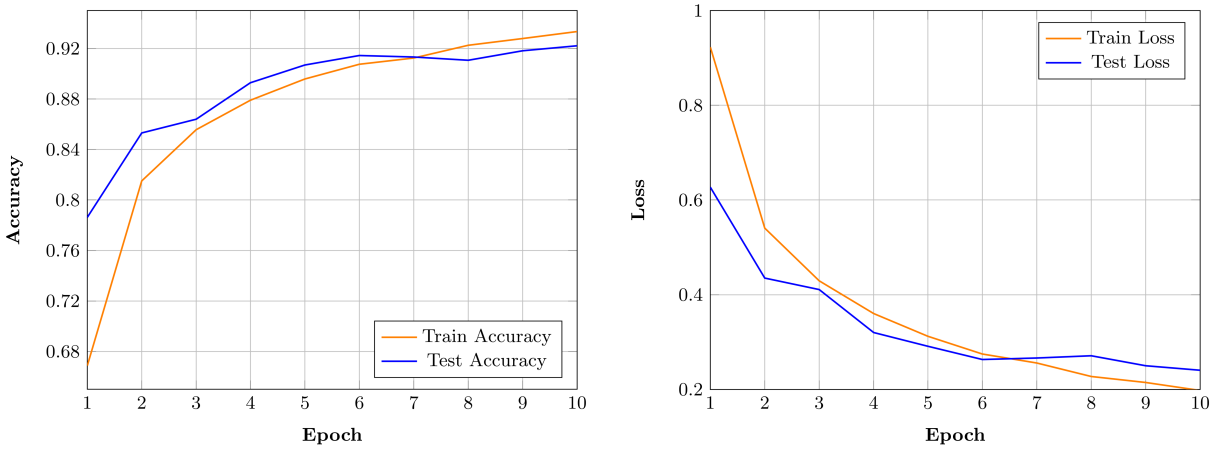

(a) Train and Test Accuracy

(b) Train and Test Loss

Figure 3: Training and validation accuracy and loss curves of the HQCNN model over 10 epochs of HQCNN on PathMNIST dataset.

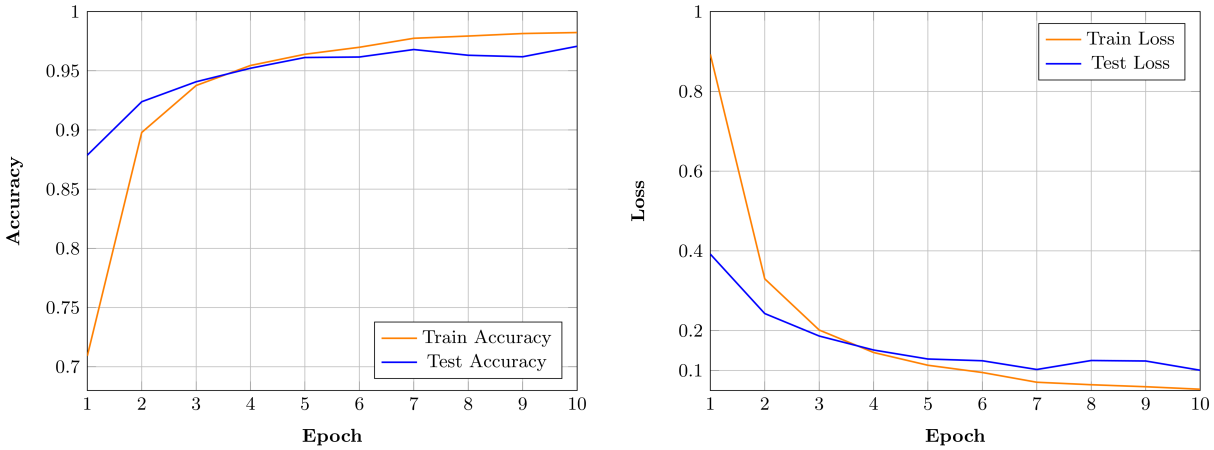

(a) Train and Test Accuracy

(b) Train and Test Loss

Figure 4: Training and validation accuracy and loss curves of the HQCNN model over 10 epochs of HQCNN on OrganAMNIST dataset.

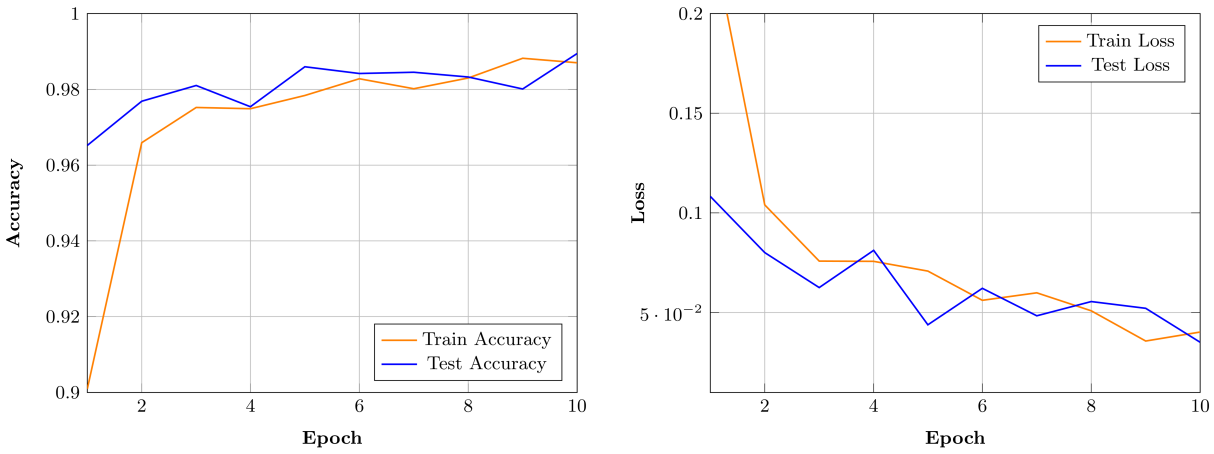

(a) Train and Test Accuracy

(b) Train and Test Loss

Figure 5: Training and validation accuracy and loss curves of the HQCNN model over 10 epochs of HQCNN on BloodMNIST dataset.

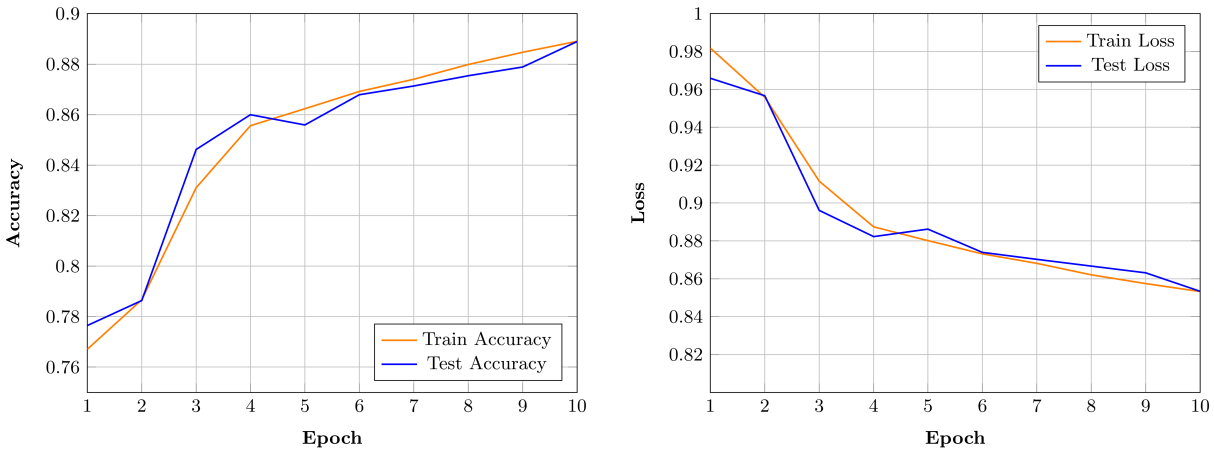

(a) Train and Test Accuracy

(b) Train and Test Loss

Figure 6: Training and validation accuracy and loss curves of the HQCNN model over 10 epochs of HQCNN on OCTMNIST dataset.

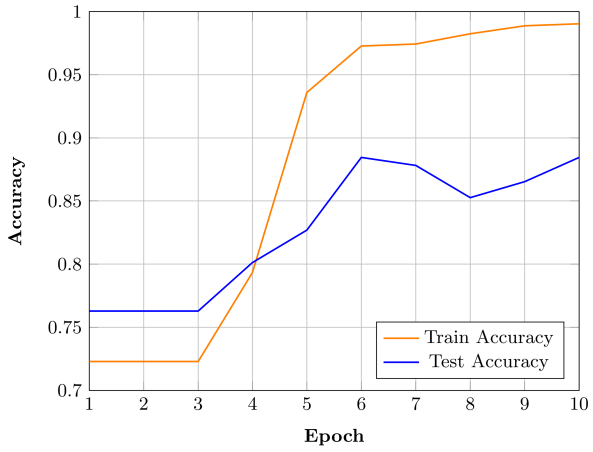

(a) Train and Test Accuracy

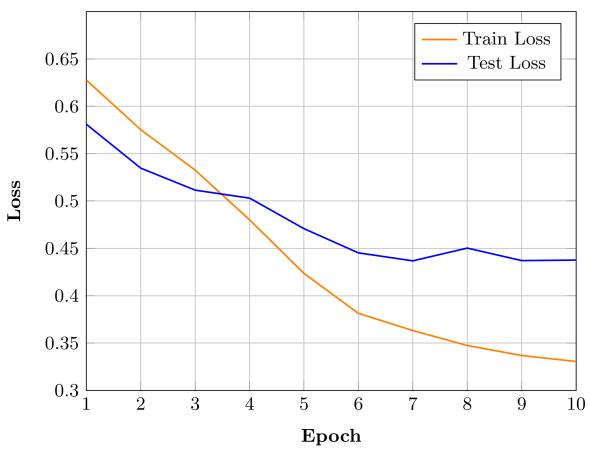

(b) Train and Test Loss

Figure 7: Training and validation accuracy and loss curves of the HQCNN model over 10 epochs of HQCNN on BreastMNIST dataset.

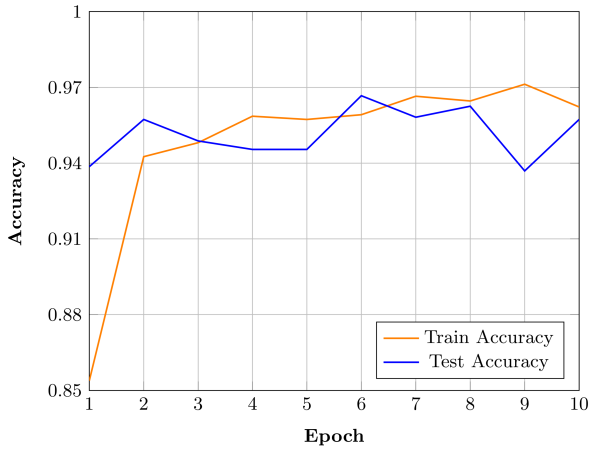

(a) Train and Test Accuracy

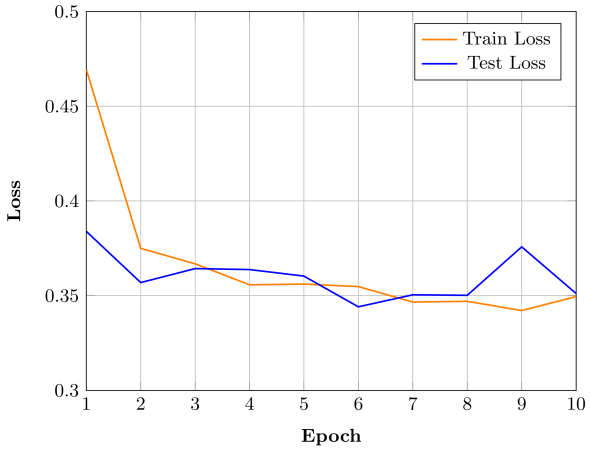

(b) Train and Test Loss

Figure 8: Training and validation accuracy and loss curves of the HQCNN model over 10 epochs of HQCNN on PneumoniaMNIST dataset.